Experimental comparison of backflow-vortex cavitation on pump inducer between cryogen and water

Y Ito, A Tsunoda, and T Nagasaki
Department of Energy Sciences, Tokyo Institute of Technology, 4259-G3-33-402 Nagatsuta-cho, Midori-ku, Yokohama, Kanagawa 226-8502, Japan

E-mail: itoyu110@00.alumni.u-tokyo.ac.jp

Abstract. The backflow-vortex cavitation on a rotating inducer was experimentally observed in both liquid nitrogen and water. The cavitation appeared "foggy" in nitrogen and "foamy" in water. This is explained by the critical Weber number theory. The number of backflow-vortex cavitation columns decreased as the head coefficient increased. This tendency is explained by a theoretical analysis in which backflow vortices are regarded as an array of vortex filaments rotating along the casing around the inducer center. The number of backflow-vortex cavitation columns is determined by the fluid dynamics and is independent of thermodynamic properties.

1. Introduction

Turbopumps for liquid-fueled rocket engines are required to be small for lightness, to suck in propellants at the minimum possible pressure to allow thin tank walls and a high payload, and to discharge propellants at the maximum possible pressure for a large thrust and a high specific impulse (ISP; with a higher ISP, a lower propellant flow rate is required for the same amount of thrust). Accordingly, a small impeller must operate at a high rotational rate; thus, cavitation is inevitable in turbopumps. The combination of an inducer (which has a low pressure ratio but resists cavitation) and a centrifugal pump (which breaks down owing to cavitation but has a high pressure ratio) is the best choice for rocket turbopumps. The inducer preliminarily compresses the working fluid and crushes the

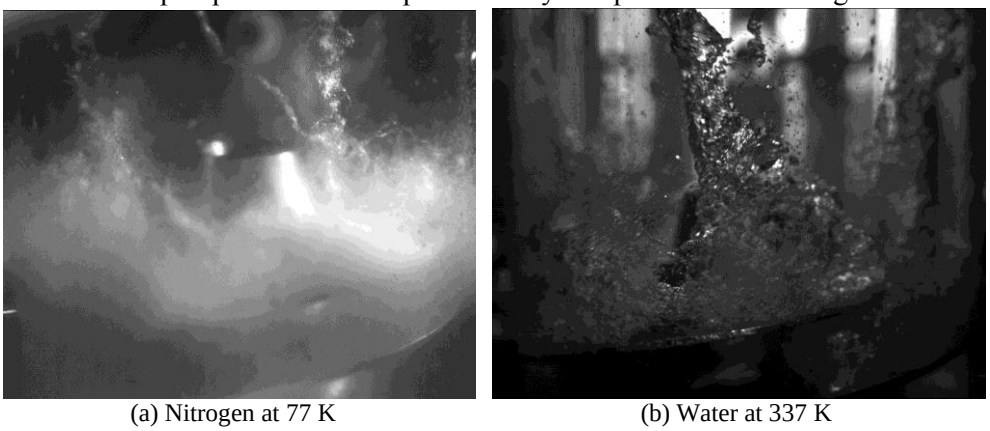

(a) Nitrogen at 77 K
$\sigma = 0.059$, $\phi/\phi_{max} = 0.47$, $\psi/\psi_{max} = 0.53$
$\omega/\omega_{ind} = 0.28$, $d/d_{ind} = 0.72$, $\delta/d_{ind} = 0.0046$

(b) Water at 337 K
$\sigma = 0.058$, $\phi/\phi_{max} = 0.45$, $\psi/\psi_{max} = 0.55$
$\omega/\omega_{ind} = 0.29$, $d/d_{ind} = 0.69$, $\delta/d_{ind} = 0.10$

Figure 1. Comparison of backflow-vortex cavitation on inducer between liquid nitrogen and water.

cavitation. Then, the centrifugal pump boosts the pressure in one shot. However, the inducer pump head abruptly fails at a very low cavitation number, σ. To effectively use the inducer, it is necessary to allow controllable cavitation to form.

Although many types of cavitation have been observed on inducers, this study focused on backflow-vortex cavitation, which is shown in Figures 1 and 2. Backflow-vortex cavitation often occurs in practical rocket turbopumps. It not only causes oscillating flows on the inducer but also affects the inducer performance. The backflow-vortex cavitation on an inducer inlet was experimentally observed by Acosta [1]. Subsequently, Aoki and Yamamoto [2], Tsujimoto et al. [3], and Yokota et al. [4] focused their research on water backflow-vortex cavitation.

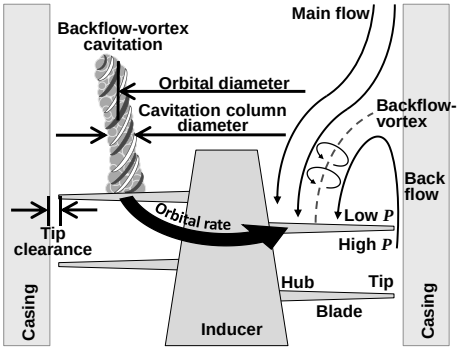

Figure 2. Schematic of backflow-vortex cavitation.

High-performance rocket engines use cryogens as propellants. Cryogens have "thermodynamic effects" whereby the temperature around the cavitation decreases because of latent heat removal, followed by a decrease in the saturation pressure and the suppression of additional cavitation. These effects decrease σ at the cavitation inception, decrease σ at the cavitation breakdown, and improve the pump head at low σ compared with room-temperature water. The consequences of the thermodynamic effects were reported by Stahl and Stepanoff [5] for hot water. Later, they were confirmed by Salemann [6], Stepanoff [7], Spraker [8], Meng [9], Ball et al. [10], Ruggeri and Moore [11], Franc et al. [12], Watanabe et al. [13], and Ito et al. [14, 15]. Ball et al. [10], Watanabe et al. [13] and Ito et al. [14, 15] visualized the cryogenic cavitation on a rotating inducer. However, there have been very few studies of the thermodynamic effects on backflow-vortex cavitation, although such cavitation may cause phenomena whereby the thermodynamic effects improve the pump performance.

Ito et al. [16] used a visualization facility to compare the backflow-vortex cavitation on a rotating inducer in liquid nitrogen with that in water. They reported that the orbital rotational rate, orbital rotational diameter, and diameter of each backflow-vortex cavitation column were determined by the head coefficient, and that among these, only the diameter of each backflow-vortex cavitation column was affected by thermodynamic effects. In the present paper, we report quantitative measurements of the number of backflow-vortex cavitation columns using the same facility as [16] and investigate whether the thermodynamic properties affect the number of backflow-vortex cavitation columns.

2. Experimental Results and Discussion

2.1. Comparison of backflow-vortex cavitation on inducer between liquid nitrogen and water

Figure 1 compares the backflow-vortex cavitation in liquid nitrogen at 77 K with that in water at 337 K under the same condition as Ito et al. [16] but at a different timing. The cavitation in nitrogen exhibits finer bubbles, i.e., cavities, compared with that in water. According to Sarosdy and Acosta [17], the cavitation behind a disk in water was "clear and well defined," and that in Freon was "indistinct and frothy." Freon, like cryogen, has a strong thermodynamic effect; thus, nitrogen cavities are similar to Freon cavities. Later, in 1965, Gadd and Grant [18] visualized the cavitation behind a disk in water, reporting that a very sharp edge yielded a "glassy clear" cavity and a dull edge yielded a "rough and striated frosted-glassy" cavity. In 1967, Ball et al. [10] visualized the cavitation around a rotating inducer in liquid hydrogen. Unfortunately, although a "foggy" cavitation is observed in their visualization photos, they reported nothing about the appearance of the cavitation in hydrogen. In 2004, Franc et al. [12] visualized the cavitation around a rotating inducer in Freon (R114). In their photos, the sheet cavitation due to the leading edge on the inducer surface is white. This probably means that the sheet cavitation is a cavity with a rough and striated surface or that it comprises small bubbles. In photos obtained using reflected light, the rough and curved surfaces are whiter, and the smooth and planar surfaces are blacker. Thus, the cavitation in Freon observed by Franc et al. exhibited similar features to that observed by Sarosdy and Acosta [17]. Yoshida et al. [19] compared the cavitation

around a rotating inducer in liquid nitrogen observed by Watanabe et al. [13] with that in water at the same cavitation number, rotational rate, and flow rate. They described the cavitation in nitrogen and water as "creamy" and "icy," respectively. Nonetheless, according to Figure 1, the cavitation in nitrogen and water is better described as "foggy" and "foamy," respectively. Cavitation bubbles are generated by shears between the backflow and blade tip and are transported to the backflow-vortex region, as shown in Figure 2. To describe the stable sizes of the cavitation bubbles, D_{Bmax}, Ito et al. [16] introduced the critical Weber number, $\mathrm{We_c}$, as

$$D_{Bmax}=\mathrm{We_c}\frac{s_L}{U^2\rho_L}, \quad (1)$$

where s_L is the surface tension, U is the local velocity, and ρ_L is the density. Here D_{Bmax} for nitrogen is 1/4 of that for water. The smaller bubbles have a larger area per volume; thus, they allow better heat transfer during growth and extinction. This is one of the reasons why nitrogen exhibits stronger thermodynamic effects than water. Furthermore, the nitrogen cavitation easily vanishes where the pressure recovers; consequently, the nitrogen pump exhibits better performance than water under low-σ operation.

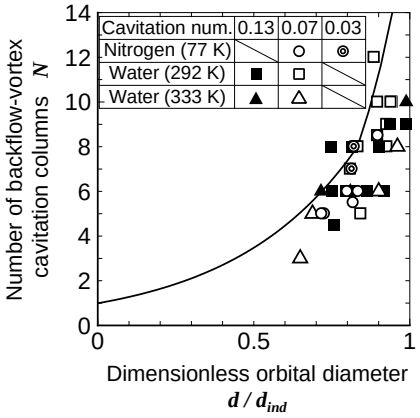

Figure 3. Number of backflow-vortex cavitation columns versus orbital diameter.

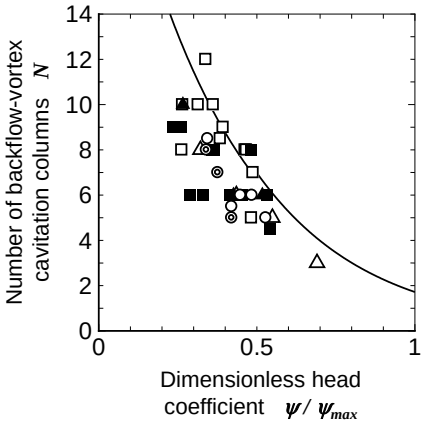

Figure 4. Number of backflow-vortex cavitation columns versus head coefficient.

2.2. Number of backflow-vortex cavitation columns

At the tip region, the backflow occurred because of the pressure difference between the inducer blade surfaces, as shown in Figure 2. The backflow made a deep inroad into the main flow and was pushed back to the inducer surface by the main flow. The backflow contained a rotational-velocity component that was affected by the rotating inducer. On the other hand, the main flow had little rotational velocity. This flow was similar to the Taylor-Couette flow. At the contact surface between the backflow and the main flow, a shear flow was formed that generated a backflow-vortex. The backflow-vortex rotated around itself in the same rotational direction as the inducer, and the orbital rotation also had the same direction as the inducer because the outer flow was faster than the inner flow.

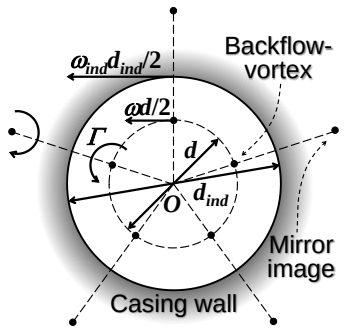

Figure 5. Theoretical model for backflow-vortices (e.g. N = 5)

The number of backflow-vortex cavitation columns was investigated. Figure 3 shows the relation between the number of backflow-vortex cavitation columns, N, and the dimensionless orbital diameter, d. N increased as d approached unity. On the other hand, Figure 4 shows the relation between N and the dimensionless head coefficient, ψ. Here, to clarify how to determine N, a theoretical analysis is conducted, as shown in Figure 5. The backflow-vortices are regarded as an array of vortex filaments rotating along the casing wall around the center of the inducer. Yokota et al. [4] conducted a stability analysis of this system; however, we did not. This is because each backflow-vortex is always generated by a shear of the Taylor-Couette flow that is different from that of the Karman vortex flow. Therefore, an array of vortex filaments can exist if the flow is physically admissible. The circulation Γ of each backflow-vortex around itself was assumed as

$$\Gamma=\pi\omega_{ind}d_{ind}^2\left\{1-(\omega/\omega_{ind})(d/d_{ind})\right\}\left\{1-(d/d_{ind})\right\}/8, \quad (2)$$

where ω is the experimental rotational rate of the backflow-vortices around O. According to [16], the relation among ω, d, the inducer rotational rate, ω_{ind}, and the inducer diameter, d_{ind}, is

$$(\omega/\omega_{ind}) = 1.36\left\{1-(d/d_{ind})\right\}^{1.49} + 0.119 . \quad (3)$$

In Figure 5, the rotational rate, ω', of each backflow-vortex around O by all of the other vortices is theoretically calculated as follows:

$$\left(\frac{\omega'}{\omega_{ind}}\right) = \frac{1}{4(d/d_{ind})}\left\{1-\left(\frac{\omega}{\omega_{ind}}\right)\left(\frac{d}{d_{ind}}\right)\right\}\left\{1-\left(\frac{d}{d_{ind}}\right)\right\}\left\{\frac{N-1}{2}\frac{1}{(d/d_{ind})} + \frac{(d/d_{ind})}{1-(d/d_{ind})^2} - \sum_{n=1}^{N-1}\frac{(d/d_{ind})^3-(d/d_{ind})\cos(2\pi n/N)}{(d/d_{ind})^4-2(d/d_{ind})^2\cos(2\pi n/N)+1}\right\} \quad (4)$$

In cases where the ω' indicated by Equation (4) equals the ω indicated by Equation (3), an array of backflow-vortices is physically admissible. The curves in Figures 3 and 4 show splines of these discrete solutions. According to Equation (3), as d increases, ω decreases; thus, a larger N is derived at a larger d from Equation (4), as shown by the curve in Figure 3. As indicated by [16], as ψ increases, d decreases and ω increases; therefore, a smaller N is derived at a higher ψ, as shown by the curve in Figure 4. Both figures indicate that the cavitation number and the type of fluid hardly affected N. This suggests that N is determined by the fluid dynamics and independent of thermodynamic properties.

3. Conclusions

The backflow-vortex cavitation on a rotating inducer was experimentally observed in both liquid nitrogen and water. The results are as follows:

– The cavitation appeared "foggy" in nitrogen and "foamy" in water. This is explained by the critical Weber number theory.

– The number of backflow-vortex cavitation columns decreased as the head coefficient increased.

– The number of backflow-vortex cavitation columns was independent of thermodynamic properties. This is explained by a theoretical analysis of the backflow-vortex cavitation.

4. References

[1] Acosta A J 1958 *2nd Symposium on Naval Hydrodynamics*, 533
[2] Aoki M and Yamamoto K 1992 *ASME J. of Turbomachinery* **114** 392
[3] Tsujimoto Y, Yoshida Y, Maekawa Y, Watanabe S and Hashimoto T 1997 *ASME J. of Fluids Engineering* **119** 775
[4] Yokota K, Kurahara K, Kataoka D, Tsujimoto Y and Acosta A J 1999 *JSME International J. Series B* **42** 451
[5] Stahl H A, Stepanoff A J and Phillipsburg N J 1956 *Transactions of ASME* 1691
[6] Salemann V 1959 *ASME J. of Basic Engineering* **81** 167
[7] Stepanoff A J 1961 *ASME J. of Engineering for Power* **83** 79
[8] Spraker W A 1965 *ASME J. of Engineering for Power* **87** 309
[9] Meng P R 1968 NASA TN D-4423
[10] Ball C L, Meng P R and Reid L 1969 NASA TM X-1360
[11] Ruggeri R S and Moore R D 1969 NASA TN D-5292
[12] Franc J P, Rebattet C and Coulon A 2004 *ASME J. of Fluids Engineering* **126** 716
[13] Watanabe M, Nagaura K, Hasegawa S, Niiyama K, Yoshida Y and Sugita E 2010 JAXA RM-09-010
[14] Kurishita Y, Ito Y and Nagasaki T 2012 *Asian Joint Conference on Propulsion and Power 2012*, AJCPP2012-093
[15] Ito Y, Kurishita Y, Kitano S and Nagasaki T 2012 *The 8th International Symposium on Cavitation*, CAV2012 No.104
[16] Ito Y, Tsunoda A, Kurishita Y, Kitano S and Nagasaki T 2015 "Experimental Visualization of Cryogenic Backflow Vortex Cavitation with Thermodynamic Effects" *AIAA J. of Propulsion and Power*.
[17] Sarosdy L R and Acosta A J 1961 *ASME J. of Basic Engineering* 399
[18] Gadd G E and Grant S 1964 *J. of Fluid Mechanics* **23** 645
[19] Yoshida Y, Kikuta K, Niiyama K and Watanabe S 2012 *ASME Fluids Engineering Summer Meeting*, FEDSM2012-72212

Acknowledgments

This work was financially supported by the Iwatani Naoji Foundation and the JAXA's Engineering Digital Innovation (JEDI) Center. The authors thank Professor Emeritus Toshio Nagashima at the University of Tokyo, who provided advice. The authors also thank Mr. Ichiro Takaki at Tokyo Institute of Technology, who selected additional data from experimental movies.